Semi-automated quantitative evaluation of neuron developmental morphology *in vitro* using the change-point test

Ashlee S. Liao [0000-0002-1828-8773][1], Wenxin Cui [0000-0002-0887-2933][1,2], Yongjie Jessica Zhang [0000-0001-7436-9757][1,2] and Victoria A. Webster-Wood [0000-0001-6638-2687][1,2,3*]

[1]Mechanical Engineering Department, Carnegie Mellon University, 5000 Forbes Avenue, Pittsburgh, 15213, Pennsylvania, United States of America.

[2]Biomedical Engineering Department, Carnegie Mellon University, 5000 Forbes Avenue, Pittsburgh, 15213, Pennsylvania, United States of America.

[3]McGowan Institute for Regenerative Medicine, University of Pittsburgh, 4200 Fifth Avenue, Pittsburgh, 15260, Pennsylvania, United States of America.

*Corresponding author(s). E-mail(s): vwebster@andrew.cmu.edu;
Contributing authors: ashleel@andrew.cmu.edu; wenxincu@andrew.cmu.edu; jessicaz@andrew.cmu.edu;

Abstract

Neuron morphology gives rise to distinct axons and dendrites and plays an essential role in neuronal functionality and circuit dynamics. In rat hippocampal neurons, morphological development occurs over roughly one week *in vitro*. This development has been qualitatively described as occurring in 5 stages. Still, there is a need to quantify cell growth to monitor cell culture health, understand cell responses to sensory cues, and compare experimental results and computational growth model predictions. To address this need, embryonic rat hippocampal neurons were observed *in vitro* over six days, and their processes were quantified using both standard morphometrics (degree, number of neurites,

total length, and tortuosity) and new metrics (distance between change points, relative turning angle, and the number of change points) based on the Change-Point Test to track changes in path trajectories. Of the standard

morphometrics, the total length of neurites per cell and the number of endpoints were significantly different between 0.5, 1.5, and 4 days *in vitro*, which are typically associated with Stages 2-4. Using the Change-Point Test, the number of change points and the average distance between change points per cell were also significantly different between those key time points. This work highlights key quantitative characteristics, both among common and novel morphometrics, that can describe neuron development *in vitro* and provides a foundation for analyzing directional changes in neurite growth for future studies.

Keywords: Neuron, Morphogenesis, Morphometrics, Change-Point Test, Developmental Growth Stages

1 Introduction

Mature neurons exhibit extensive arborization of their axons and dendrites (collectively neurites) to form functional connections with neighboring cells and receive sensory signals. The distinct neuronal structure is believed to give rise to the neuron's computational abilities (Cuntz, Borst, & Segev, 2007; Ferrante, Migliore, & Ascoli, 2013; Kanari et al., 2018; van Elburg & van Ooyen, 2010; Zomorrodi, Ferecsk´o, Kov´acs, Kr¨oger, & Timofeev, 2010). In addition, morphological differences between neuronal cell types are thought to result in their functional differences (Khalil, Farhat, & Dl otko, 2021; Krichmar, Nasuto, Scorcioni, Washington, & Ascoli, 2002; Mainen & Sejnowski, 1996; Schaefer, Larkum, Sakmann, & Roth, 2003; Vetter, Roth, & H¨ausser, 2001). During the development of this crucial structure in primary neurons *in vitro*, several morphological changes have been categorized into distinct stages which can be described qualitatively (Dotti, Sullivan, & Banker, 1988; Powell, Rivas, Rodriguez-Boulan, & Hatten, 1997; Tahirovic & Bradke, 2009).

One common model for studying neuron morphological development *in vitro* is the embryonic rodent hippocampal neuron (Tahirovic & Bradke, 2009). In this model system, morphogenesis of hippocampal neurons can be qualitatively described in five developmental stages occurring over seven days *in vitro* (DIV) (Figure 1): initially, neurons appear as only round somas with no neurites, but (1) within the first hour of plating, small protrusions, or lamellipodia, form along the cell periphery; (2) after around 0.5 days *in vitro* (DIV), the lamellipodia transforms into a few distinct, minor processes that form the preliminary neurites; (3) at around 1-2 DIV, one of the neurites will begin to elongate at a faster rate than the other processes and differentiate into the axon; (4) after 4 DIV, the remaining neurites will develop into dendrites and begin to elongate at a higher rate, but still slower than that of the axons; (5) after one week in culture, the neuronal processes will continue

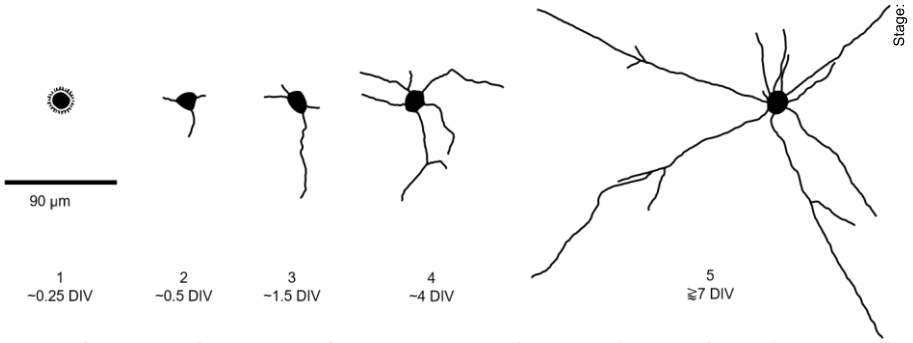

Fig. 1 Rat hippocampal neuron morphogenesis occurs in five stages (Dotti et al., 1988). First, small protrusions, or lamellipodia, form at the soma boundary (Stage 1). Subsequently, a few lamellipodia will continue to elongate into the initial neurites (Stage 2). Next, one of the neurites will begin to grow faster than the others to differentiate into the axon (Stage 3). After a few days, the remaining neurites will also accelerate growth to mature into the dendrites (Stage 4). The final stage is the continued maturation of the entire cell, which is dependent on environmental factors and interactions with neighboring cells (Stage 5).

to mature by forming networks with functional synaptic connections, and the dendrites will begin to exhibit dendritic spines (Dotti et al., 1988; Kaech & Banker, 2006; Tahirovic & Bradke, 2009). Previously, each stage has been qualitatively described with limited quantitative descriptions of the axonal and dendritic lengths and growth rates (Dotti et al., 1988). However, it can be challenging to identify the stage a culture is at using only those features, particularly when transitioning between stages if the same cells within a population were not tracked over time. Nevertheless, these stages are still used as expected growth events when assessing *in vitro* cultures (Kaech & Banker, 2006). Neurite growth quantification is needed for consistent stage identification to monitor culture health, test intra- and extracellular sensory cues, and compare experiments and computational models (Liao, Webster-Wood, & Zhang, 2021; Qian et al., 2022).

Many different types of quantitative representations, such as density maps (Jefferis et al., 2007; Laturnus, Kobak, & Berens, 2020), graph theory (Gillette & Grefenstette, 2009; Heumann & Wittum, 2009), topology (Kanari et al., 2018), and morphometric statistics (Laturnus et al., 2020; Polavaram, Gillette, Parekh, & Ascoli, 2014; Uylings & van Pelt, 2002), have been applied to describe functionally different types of mature neurons. In addition, machine learning techniques also have been used for identifying neuron types (Laturnus et al., 2020) and for identifying neuronal polarity (Su et al., 2021). Laturnus et al. (2020) noted the importance of the spatial extent and shape describing neuron connectivity in distinguishing cell types, instead of specific branching features. Although these quantitative representations can characterize neuronal cell types, most have not been applied to discriminate between neurite growth stages or time points. A few common morphometrics, such as neurite length and number of branches, have been used to study neuron development *in vitro* in rat hippocampal neurons (Dotti et al., 1988) and in stem cell differentiation to

neural progenitor cells (Kang et al., 2017). However, the current quantitative representations of neuron morphology do not capture details about changes in neurite growth direction, which can change in response to chemotropic molecules in the surrounding environment and from cell-to-cell signaling (Bicknell, Pujic, Dayan, & Goodhill, 2018; Deinhardt et al., 2011; Ferreira Castro et al., 2020; Tamariz & Varela-Echavarr´ıa, 2015).

To characterize the stages of neuron growth *in vitro* and quantitatively capture changes in neurite growth direction, we created a semi-automated tool to systematically analyze the development of neurons. We applied this tool to assess the development of rat hippocampal neurons *in vitro*. Based on qualitative observations of neurons growing *in vitro*, we hypothesized that the number of substantial changes in growth direction and the distance between such changes varies between developmental stages. To test this hypothesis our semi-automated tool performs quantitative analysis using both common morphometrics used to describe mature neurons (Laturnus et al., 2020) and new morphometrics based on analysis using a Change-Point Test (CPT) (Byrne, Noser, Bates, & Jupp, 2009; Liao et al., 2021). The CPT implemented was originally developed to identify locations along an animal walking path in which the direction was changed towards a resource of interest (Byrne et al., 2009). As such, this method allows a trajectory to be analyzed to identify locations of significant directional change and the distance between these changes. Using the CPT, our tool calculates the number of change points along a traced neurite trajectory, the distance between change points, and the turning angle at each change point. In this work we present the generation of a model *in vitro* neuron growth dataset, an image processing workflow to prepare and trace images for analysis, and our method for automatic morphometric evaluation of neurite features. Finally, we assess the ability of each calculated morphometric to act as an indicator of neuron growth stage *in vitro* using our model data set.

2 Methods

2.1 Data Set Generation

A data set, comprised of images of primary rat hippocampal neurons cultured over 6 DIV and the resulting neurite traces, was created to characterize neuron morphogenesis. To generate this data set, images of *in vitro* neurons were obtained using inverted bright-field microscopy and then processed using NeuronJ (Meijering et al., 2004) to obtain traces of each developing neurite on a cell (Figure 2) (Liao et al., 2021).

2.1.1 Cell Culture

Cryopreserved primary, embryonic-day 18 (E18) rat hippocampal neurons (A36513, Gibco, USA) were thawed and plated in 48-well plates (150687, Nunc, USA) that were coated in poly-D-lysine (P6407, Sigma-Aldrich, USA), as per

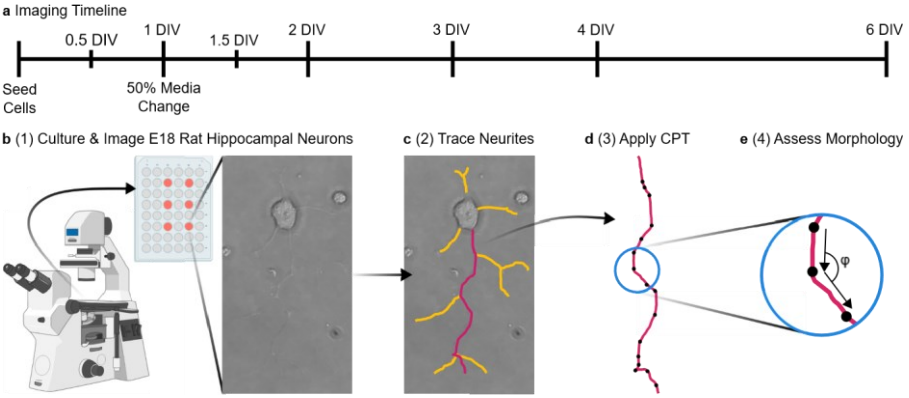

Fig. 2 There are four major steps for the methods workflow. (a-b) In the first step, cryopreserved embryonic day 18 (E18) primary rat hippocampal neurons were thawed, cultured, and monitored using inverted bright-field microscopy over six days *in vitro* (DIV) . The microscope and well plate diagram was created with BioRender.com. (c) In the second step, images of the neurites were traced using NeuronJ and then (d) quantified using the CPT. (e) Lastly, using the neurite traces and CPT results, selected morphometrics (Figure 3) were measured and statistically analyzed using the Anderson-Darling test, Kruskal-Wallis test, and the Dunn test with a Bonferroni correction.

manufacturer's protocol (Thermo Fisher Scientific, 2018). Briefly, the plate was treated with 50 μg/mL poly-D-lysine (P6407, Sigma-Aldrich, USA) and incubated at room temperature for 1 hour before being rinsed with sterile, deionized water. Once dry, the plates were wrapped with Parafilm (BM999, Bemis, USA) and stored overnight in a refrigerator (2-8°C). After the wells were treated, the neurons were seeded at a density of 10,000 cells/cm^2 in Neurobasal Plus (A3582901, Gibco, USA) supplemented with 2% B-27 Plus (A3582801, Gibco, USA). The low densities allowed more neurites to be identified and traced before their arborization became too dense to distinguish individuals using bright-field microscopy. The cultures were incubated at 37°C and 5% CO_2, except during media changes and imaging periods. Twenty-four hours after initial seeding, 50% of the media was replaced with fresh media. The cultures were imaged using a 12 megapixel color camera on an Echo Revolve microscope in the inverted configuration and using the bright field setting at 20X or 40X magnification, depending on whether entire cells with their full neurite trees could be captured in a single image, during the following time points (DIV): 0.5, 1, 2, 3, 4, 6 (Figure 2).

2.1.2 Image Processing Workflow using Semi-Automated Tracing

Neurites identified in the images were semi-automatically traced using NeuronJ (Meijering et al., 2004), a plugin in ImageJ (Rueden et al., 2017; Schindelin et al., 2012). All neurons included in the dataset had broad, flat somas with at least one distinct projection. These inclusion criteria ensured that the neurons had adhered to the surface of the plate and are an indication of good culture

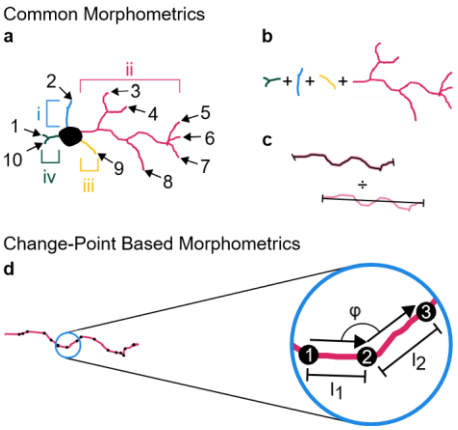

Fig. 3 Seven metrics were used to characterize neurite morphogenesis. Among the common morphometrics, there were four features: (a) degree or the number of endpoints for a given cell represented by the black arrows with Arabic numerals, number of neurites for a given cell represented by the colored brackets with Roman numerals, (b) total length of the cell or the sum of the lengths of all of its neurites, and (c) tortuosity of a neurite, which is the total path length divided by the shortest distance from its endpoints. The average tortuosity of the cell was assessed in this work. (d) In addition, a novel application of the CPT led to three new features: distance between change points indicated by l_1 and l_2, number of change points represented by the numbered black circles, and relative turning angle defined by ϕ.

conditions (Kaech & Banker, 2006). In addition, to be included in the data set, all of a cell's projections had to be visible within a single image, ensuring that the whole cell was captured. Overlapping neurites were excluded if their paths were not clear to prevent assigning neurites to the wrong cell or not fully tracing a neurite path. After all of the neurites on a cell were traced (Figure 2c), the coordinates of each neurite trace were exported out of NeuronJ as text files to be automatically evaluated for their features. In addition, metadata detailing which cell each neurite trace belonged to were exported from NeuronJ as a comma-separated values (CSV) file. For the morphometric analyses, each neuron cell was characterized by all of its neurite projections (traces).

2.2 Automatic Morphometric Evaluation of Neurite Features

After the data set was generated, the features of the developing neurites were analyzed using the CPT and quantified using both select common neuron morphometrics and novel morphometrics derived from the CPT results (Figures 2c, 2d, 3). The text files detailing each neurite trace were processed using R (https://www.r-project.org/, version 4.1.2) (R Core Team, 2021) within RStudio (RStudio Team, 2021). The subsequent statistical analyses were completed using R (https://www.r-project.org/, version 4.1.2) (R Core Team, 2021). The violin plot distributions were generated using the seaborn package (Waskom, 2021) in Python 3.7.6 (Python Core Team, 2021) using Jupyter Notebook 6.0.3 (Kluyver, Ragan-Kelley, P´erez, & Granger, 2016).

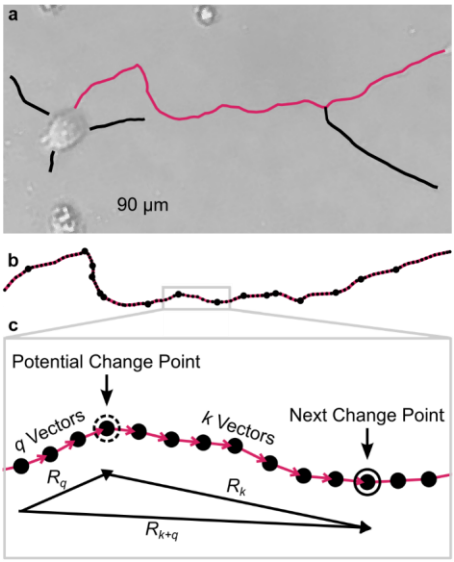

Fig. 4 The CPT was run on each neurite trace to identify novel morphometrics to describe the changes in neurite path directions. (a) First, the neurites are traced and the pixel coordinates describing the path were exported from NeuronJ. (b) For example, in the magenta trace, the small dots represent each pixel coordinate, and the large dots represent the change points identified using the CPT by Byrne et al. (2009). (c) Briefly, k number of vectors are formed between the coordinates (filled circles) of the last known change point or the initial end point of the trace (solid ring, "Next Change Point") and the coordinate point being assessed (dashed ring, "Potential Change Point"). The user is allowed to select q number of vectors that occur before the Potential Change Point. To assess the collinearity, $R_q + R_k$ is compared with R_{k+q} using a permutation test (Byrne et al., 2009; Conover, 1971).

2.2.1 Common Morphometrics

Four common morphometrics were selected to characterize neurite development (Figure 3a-c): number of neurites, degree, total length per cell, and average tortuosity per cell (Kang et al., 2017; Laturnus et al., 2020; Polavaram et al., 2014; Uylings & van Pelt, 2002). An R script was generated to calculate these features automatically based on the trace information. For each cell, degree and number of neurites were counted. The lengths of all of the neurite traces per cell were summed to calculate the total length. For each neurite trace, the length was calculated by adding the distance between consecutive coordinate points. The fourth metric, tortuosity, was calculated by taking the length of a given trace and dividing it by the distance between its two endpoint coordinates. The tortuosity was averaged for each cell.

2.2.2 Novel Morphometrics Based on a Change-Point Test

The traces were also analyzed using a Change-Point Test to assess points of significant directional change. We selected the CPT presented by Byrne et al. (2009) because it determines changes in path direction by assessing the collinearity of segments along the entire trajectory. This CPT was used initially

for identifying locations of significant directional changes in animal walking trajectories. For a full mathematical description, readers are encouraged to refer to the original work of Byrne et al. (2009). Briefly, the original CPT took an input of GPS data of animal travel routes and, using a permutation test (Conover, 1971), analyzed the collinearity of vectors created between subsequent coordinate points (Figure 4) (Byrne et al., 2009). The original R script presented by Byrne et al. (2009) was transformed into a callable function to process the neurite traces, represented by pixel coordinate points exported from NeuronJ. In addition to the coordinate data, the CPT requires the user to select a significance level and the number of consecutive vectors to assess for collinearity when searching for a change point (Figure 4). Using a significance level of 0.05, we applied the CPT to each neurite trace for q vectors prior to the potential change point. To determine q, the semi-automated tool performs the CPT over all integer q values from $q = 1$ to $q = 10$. Each time the CPT is conducted, the tool stores the number of change points determined for that q. Following the procedure described in Byrne et al. (2009), the tool selects and saves the results that produce the largest number of change points. If multiple q values result in the maximum number of change points, the CPT result requiring the smallest q is selected for further processing.

Using the change points identified by the CPT, three additional neurite morphometrics were defined (Figure 3d): the number of change points, segment length, and relative turning angle. An R script was generated to automatically calculate these features based on the CPT results and the trace information. The number of change points was summed per cell as a single metric. Another metric, segment length, was defined to be the distance between two consecutive change points. Segment length was calculated by summing the distances between coordinate points between two consecutive change points. Lastly, the relative turning angle was defined as the angle measured between two consecutive segment lengths between 0°and 180°.

2.3 Statistics

Distributions of each morphometric were first tested for normality using the Anderson-Darling test (Gross & Ligges, 2015). All distributions were determined to be non-normal, and therefore, non-parametric analyses were used. The Kruskal-Wallis test (R Core Team, 2021) was first used to determine whether there are any significant changes between imaging time points for each feature. A post-hoc Dunn test with a Bonferroni correction (Dinno, 2017) was used to follow up with multiple pairwise comparisons. A significance level (α) of 0.05 was used for the analysis. For the Kruskal-Wallis test, the null hypothesis was reject based on $p \leq \alpha$ (R Core Team, 2021). For the Dunn test, the null hypothesis was rejected based on $p \leq \alpha/2$ (Dinno, 2017).

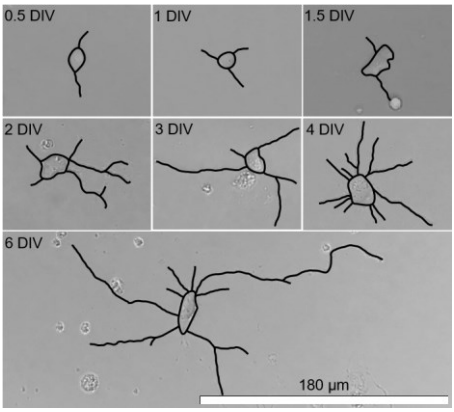

Fig. 5 Over 6 DIV, rat hippocampal neurons progress through roughly four developmental stages. The length and number of neurites and bifurcations have notable changes, which are statistically represented in Figure 8.

3 Results

3.1 Data Set

The data set generated is comprised of three types of data (Figure 5): microscope images of neurons at seven time points, the associated traces for those neurons that met the tracing criteria (Section 2.1.2), and the resulting morphometrics (both common and new). The seven time points were selected to observe the neurons undergo three key growth stages (Figures 1 and 5): 0.5 DIV (estimated Stage 2, n = 31 cells), 1 DIV (n = 36 cells), 1.5 DIV (n = 80 cells), 2 DIV (n = 135 cells), 3 DIV (n = 234 cells), 4 DIV (n = 162 cells), and 6 DIV (n = 20 cells). This data is available at https://doi.org/10.5281/zenodo.6415473.

3.2 Common Metrics Performance

Several of the common metrics typically used for quantifying neuron morphology showed a significant ability to discriminate between growth time points. The Kruskal-Wallis test indicated that the medians were significantly different in at least one time point for all four common morphometrics assessed. In particular, using the Dunn test, the total length of all neurites, the degree, and the number of neurites were significantly different between several pairs of time points (Figure 8). For the time point typically associated with Stage 4 (4 DIV), total length, degree, and number of neurites were significantly different from the Stage 2 and 3 time points (0.5 and 1.5 DIV, respectively) (total length and degree highlighted in Figure 6). However, the features were not significantly different between 0.5 and 1.5 DIV (Figure 6). Average tortuosity was only significantly different between 1.5 and 3 DIV (Figure 8).

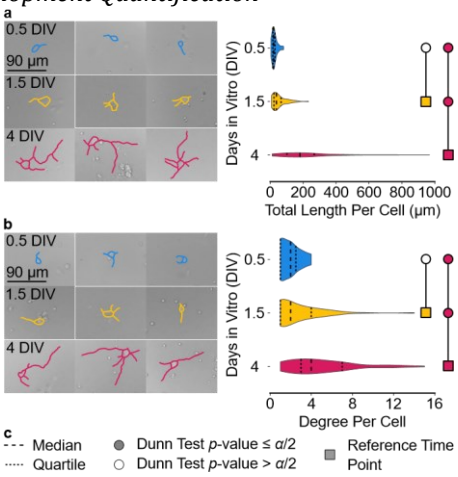

Fig. 6 Of the common morphometrics, the (a) total length per cell and the (b) degree were among the features that best distinguished between 0.5 DIV (≈ Stage 2), 1.5 DIV (≈ Stage 3), and 4 DIV (≈ Stage 4). Representative neurons are on the left panels, while the distributions are on the right. The median, upper and lower quartiles, and significance from each statistical test for each feature shown in the violin plots (a-b) are represented by the symbols in the legend (c). The Dunn test with a Bonferroni correction indicated that total length and degree were significantly different between 0.5 DIV and 4 DIV and between 1.5 DIV and 4 DIV.

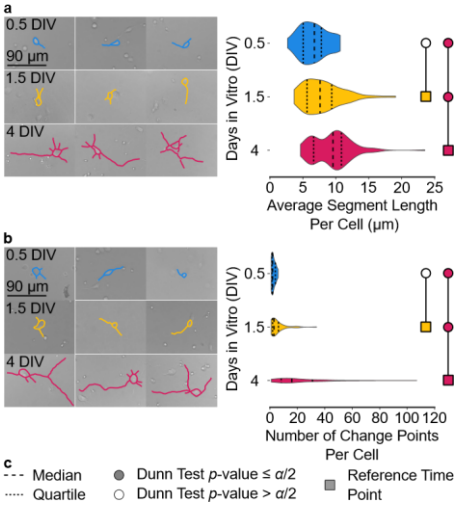

Fig. 7 From the novel CPT-Based morphometrics, the (a) average segment length and the (b) number of change points were among the features that best distinguished between 0.5 DIV (≈Stage 2), 1.5 DIV (≈Stage 3), and 4 DIV (≈Stage 4). On the left, representative neurons with traces are shown. The distributions of each feature are on the right panels. The symbols in the legend (c) represent the medians, upper and lower quartiles, and statistical significance for each feature shown in the violin plots(a-b). The Dunn Test with a Bonferroni correction indicated that the average segment length and the number of change points were significantly different between 0.5 DIV and 4 DIV and between 1.5 DIV and 4 DIV.

3.3 Change-Point-Test-Based Novel Morphometrics Performance

Two of the three CPT-based morphometrics introduced in this work varied significantly between time points. The number of change points and average segment length were significantly different for a majority of the time point pairs (Figure 8), including time points typically associated with Stages 2-4 (Figure 7). The relative turning angle was not significantly different between any of the time points (Figure 8).

4 Discussion

Our study provides a method for the quantitative description of embryonic rodent hippocampal neurons across the first week of culture through a combination of common and CPT-based morphometrics. By characterizing a sample population of cells, the morphometrics and our presented dataset can be used in the future to assess the effects of experimental conditions in combination with the qualitative expected growth stage milestones outlined by Kaech and Banker (2006) and Dotti et al. (1988). At a population level, the distributions of total length found in our study are in alignment with the single cell values reported in Dotti et al. (1988).

When analyzing the data set at the time points associated with a specific growth stage (Figure 1), specifically 0.5 DIV (Stage 2), 1.5 DIV (Stage 3), 4 DIV (Stage 4), several features, both common and derived from the CPT, were significantly different (Figures 6-7). These differences indicate that total length, degree, segment length, and the number of change points could be used to characterize the morphological development of these neurons and possibly be used to distinguish between the associated stages. However, additional analysis would be needed to match the stages, as classified by an expert observer, with features characterized and time *in vitro*.

To quantify local changes that occur during neuron morphological development, quantitative metrics of neurite growth direction are needed. Sholl analysis (Sholl, 1953), branching angles, and tortuosity can provide a snapshot representation of the neurite spatial organization and orientation. However, they do not indicate if the difference in space or orientation is due to specific intra- or extracellular signaling or due to stochastic processes. In contrast, the CPT method (Byrne et al., 2009) applied in the presented work identifies where along a path in which a statistically significant directional change has occurred. From that information, the magnitude of the change and the specific angle can be extracted. Our study demonstrated that the CPT leads to additional morphometrics that were significantly different between key time points (Figure 7), which may indicate important directional change events during the growth stages, even in media without a controlled gradient of extracellular cues.

growth *in vitro*. For example, future experimental studies should apply the semi-automated morphological analysis presented here to assess neuron cultured in the presence of specific growth factors known to affect neuron growth and maturation, such as nerve growth factor, brain-derived neurotrophic factor, or neurotrophin-3, to investigate whether this approach can distinguish between such experimental conditions. Furthermore, because the CPT was initially developed to objectively identify where the animals decide to switch from randomly meandering to directed walking (Byrne et al., 2009), we hypothesize that in future studies, the CPT could be applied to identify changes in neurite growth direction in the presence of external cues. To test this hypothesis in future work, chemotropic molecules, such as netrins and semaphorins, could be applied at specific time points and regions to control cell growth direction to assess the ability of these morphometrics to identify cells which are undergoing directed versus undirected growth.

In addition, the automated portion of morphological analysis tool overall could be used to characterize more neuron types or neurites with a more extensive tree, as long as the neurite path can be described as a list of coordinates and a metadata file for individual trace identification (*i.e.* trace identification, the neuron cell it belongs to, and tracing type as found in the accompanying CSV file with the traces in the GitHub repository). This provides flexibility in the method of obtaining the raw data in the choice of imaging modality, cell type, and level of arborization. Future studies are needed to assess the ability of this approach to distinguish *in vivo* cell morphologies.

4.1 Limitations

This study has several limitations based on the imaging modality used for tracking the cells over time. Bright-field microscopy at 20X and 40X magnification is a method for imaging several cells over a short time-period without the potential interference of dyes that could affect the cell's structural development. Bright-field imaging can also be used to quickly assess cell health during the culturing period. However, bright-field microscopy results in a lower contrast imaging modality than fluorescence microscopy, which is more challenging for image processing techniques to extract the neurite trajectories. Furthermore, the use of only 20X or 40X magnification limited the size of the neurites we were able to capture, which affects the sample population of neurons that were analyzed. This is particularly evident in the smaller sample sizes at the earlier time points (0.5 and 1 DIV) and the latest time points (6 DIV). A higher magnification or different imaging modality may allow the smaller

features, such as lamellipodia or young neurites, to be better captured. In addition, stitching multiple images may be useful for capturing extensive, mature neurites at later stages.

The use of the bright-field imaging technique resulted in the choice of using the semi-automatic tracing program, NeuronJ (Meijering et al., 2004), to trace the neurites since many other automatic programs are optimized for highcontrast fluorescence images (Boulan et al., 2020; Ho et al., 2011; Kim, Son, & Palmore, 2015; Pool, Thiemann, Bar-Or, & Fournier, 2008). Although the semi-automatic procedure may introduce some interobserver variability, the process will still be more reproducible than a fully manual method (Meijering et al., 2004). Furthermore, due to the need for user input, the labor intensiveness of this method scales with the number of neurites. However, it is still an improvement over a completely manual method with better neurite centerline representations and negligible differences in length results (Meijering et al., 2004).

Moreover, without the use of fluorescence dyes, neurons cultured beyond 6 DIV (estimated transition point between Stage 4 and 5) become difficult to distinguish due to the development of long neurites and dense networks at Stage 5 (Kaech & Banker, 2006). Furthermore, a distinct qualitative morphological change is not present between Stage 4 and 5, and Stage 5 is likely highly influenced by other cell interactions, unlike the previous stages that are considered endogenously determined (Dotti et al., 1988). Thus, Stage 5 was not considered as part of the scope of the work presented here. Additional studies controlling the cell interactions between developing neurons would be required to characterize Stage 5 morphology based on environmental conditions using our collection of quantitative morphometrics.

There are also some limitations in the computational methods implemented. In the CPT specifically, there is a balance between the selection of the significance level and the number of vectors to be used in the collinearity assessment (Byrne et al., 2009). The smaller the number of vectors used, the more sensitive the CPT is to detecting genuine change points (Byrne et al., 2009). However, if a higher significance level is desired, a larger number of vectors may be required (Byrne et al., 2009). In addition, the statistical analysis was completed on a per cell basis (using averages and sums over an entire neuron), rather than a per neurite basis. This may result in some loss of fine details of the neurites themselves, while enabling the study of the cell morphology as a whole. Further studies using techniques, such as a timelapse imaging, could complement our semi-automatic tool in assessing culture condition effects on individual neurites. Such individual neurite analysis may be particularly important for future studies on directed neuron growth.

5 Conclusions

This study provided a semi-automated quantitative analysis method, including both common and novel morphometrics. We used this method to analyze growth during the initial 6 DIV for cultured neurons, which correspond to three of the five growth stages qualitatively described for embryonic rodent hippocampal neurons in culture. This semi-automated quantitative analysis method has many potential applications, including assessing the cell culture health and how certain intrinsic or extrinsic factors may alter neuron morphological development. The novel application of the Change-Point Test, which was initially developed for studying animal walking paths, could also provide

additional insight on factors that alter the neurite trajectories in future studies. In addition, quantifying the development of neuron morphology can inform parameters needed for computational simulations of neuron growth (Qian et al., 2022), materials transport (Li, Barati Farimani, & Zhang, 2021; Li, Chai, Yang, & Zhang, 2019), and molecular traffic jams (Li & Zhang, 2022a, 2022b). More accurate computational models could help guide future *in vitro* studies by exploring experimental parameters *in silico* prior to costly and time intensive experimentation. Finally, with our semi-automatic quantitative method for characterizing neuron morphology, experimental results can be consistently assessed by both novices and experts, and results can be easily compared across studies.

Appendix A: Distributions and Analyses on All Morphometrics for All Observed Time Points

A summary of the Dunn tests along with each feature's distributions are showcased in Figure 8. The Dunn tests with a Bonferroni correction indicated significant differences between several time points, as outlined in the corresponding Tables below, for segment length (Figure 8a, Table 10), number of change points (Figure 8c, Table 12), total length (Figure 8d, Table 13), number of neurites (Figure 8e, Table 14), and degree (Figure 8g, Table 16). No significant differences between time points were detected for turning angle (Figure 8b, Table 11), and significant differences were only detected between DIV 1.5 and 3 for tortuosity (Figure 8f, Table 15).

Additionally, the sample sizes of the data set are reported in Table 1. The summary statistics and Anderson-Darling results for all of the morphometrics are detailed in Tables 2-8. The χ^2 and p-values from the Kruskal-Wallis tests for each feature are in Table 9. Lastly, the post-hoc Dunn tests with a Bonferroni correction p-values are in Tables 10-16.

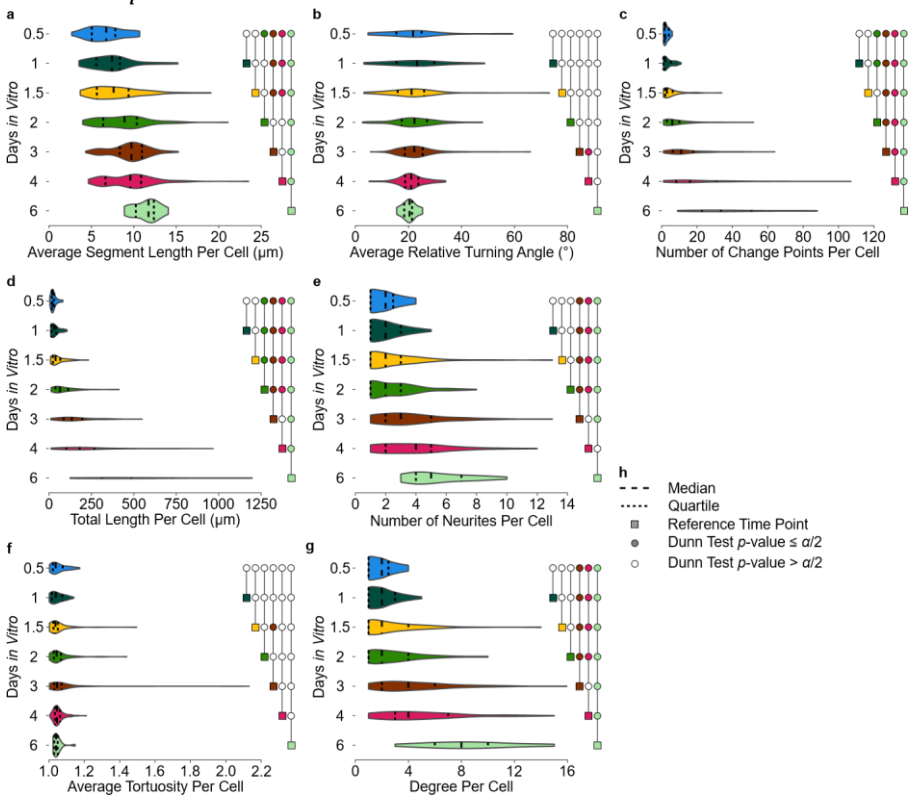

Fig. 8 The distributions and results of the Dunn test with a Bonferroni correction used to assess each morphometric (a) average segment length, (b) average relative turning angle, (c) number of change

points; (d) total length, (e) number of neurites, (f) average tortuosity, (g) degree) for every time point pair are symbolically represented, as defined in (h).

Table 1 Overall Data Set Size

DIV	Sample Size (Number of Cells)	Number of Neurites Traced
0.5	31	47
1.0	36	58
1.5	80	169
2.0	135	348
3.0	230	830
4.0	162	668
6.0	20	139

Table 2 Summary Statistics and Anderson-Darling Results for Average Segment Length Per Cell (μm)

DIV	Mean	Standard Deviation	Median	First Quartile	Third Quartile	Anderson-Darling Test Statistic	AndersonDarling p-value
0.5	6.68	2.14	6.75	5.05	7.82	0.505	0.188
1.0	7.39	2.53	7.43	5.58	8.36	0.831	0.0289
1.5	8.00	2.93	7.62	5.64	9.39	1.48	0.00075
2.0	8.82	2.93	8.90	6.39	10.35	1.15	0.00512
3.0	9.51	2.16	9.72	8.35	10.95	1.96	<0.0001
4.0	9.42	2.87	9.58	6.65	10.86	2.26	<0.0001
6.0	11.48	1.45	11.73	10.24	12.36	0.413	0.308

Table 3 Summary Statistics Anderson-Darling Results for Average Relative Turning Angle Per Cell (°)

DIV	Mean	Standard Deviation	Median	First Quartile	Third Quartile	Anderson-Darling Test Statistic	AndersonDarling p-value
0.5	22.18	11.65	21.75	15.49	25.00	1.37	0.00124
1.0	22.82	10.82	23.31	15.57	29.71	0.196	0.884
1.5	21.34	9.69	21.20	15.96	25.94	1.59	0.00039
2.0	22.32	8.01	22.32	17.51	27.06	1.07	0.00816
3.0	22.88	6.78	22.24	18.67	25.39	4.69	<0.0001
4.0	21.28	4.91	21.07	18.79	23.77	1.85	<0.0001
6.0	20.32	2.65	20.45	18.45	21.36	0.284	0.593

Table 4 Summary Statistics Anderson-Darling Results for Number of Change Points Per Cell

DIV	Mean	Standard Deviation	Median	First Quartile	Third Quartile	Anderson-Darling Test Statistic	AndersonDarling p-value
0.5	2.65	1.52	2	1.5	4	1.39	0.0011
1.0	3.56	2.97	2	1	5.25	2.52	<0.0001
1.5	5.16	5.56	3	2	6.25	7.31	<0.0001
2.0	8.22	8.24	6	3	10	7.98	<0.001
3.0	13.52	10.79	11	6.25	17.75	9.38	<0.0001
4.0	21.57	19.62	16	8.25	31	7.72	<0.0001
6.0	39.70	23.33	33.5	22.75	50.75	0.681	0.0639

Table 5 Summary Statistics Anderson-Darling Results for Total Length of All Neurites Per Cell (μm)

DIV	Mean	Standard Deviation	Median	First Quartile	Third Quartile	Anderson-Darling Test Statistic	AndersonDarling p-value
0.5	27.53	17.43	21.70	16.92	29.76	1.91	<0.0001
1.0	36.54	26.25	30.32	15.08	43.27	1.86	<0.0001
1.5	53.19	43.04	38.78	23.27	66.88	4.32	<0.0001
2.0	84.34	65.69	64.87	38.43	112.92	4.89	<0.0001
3.0	155.13	102.75	134.34	86.02	196.46	5.02	<0.0001
4.0	218.74	163.14	181.27	102.25	268.21	4.6	<0.0001
6.0	554.73	337.47	485.99	312.02	719.49	0.83	0.0264

Table 6 Summary Statistics Anderson-Darling Results for Total Number of Neurites Per Cell

DIV	Mean	Standard Deviation	Median	First Quartile	Third Quartile	Anderson-Darling Test Statistic	AndersonDarling p-value
0.5	1.94	0.998	2	1	2.5	2.16	<0.0001
1.0	2.00	1.10	2	1	3	2.36	<0.0001
1.5	2.39	2.02	2	1	3	6.6	<0.0001
2.0	2.52	1.63	2	1	3	6.97	<0.0001
3.0	3.67	2.25	3	2	5	6.41	<0.0001
4.0	3.94	2.40	4	2	5	3.4	<0.0001
6.0	5.50	2.04	5	4	7	0.907	0.0167

Table 7 Summary Statistics Anderson-Darling Results for Average Tortuosity Per Cell

DIV	Mean	Standard Deviation	Median	First Quartile	Third Quartile	Anderson-Darling Test Statistic	AndersonDarling p-value
0.5	1.0554	0.0446	1.0379	1.0225	1.0776	1.3	0.0019
1.0	1.0478	0.0363	1.0391	1.0161	1.0757	0.794	0.0359
1.5	1.0530	0.0652	1.0367	1.0254	1.0507	9.68	<0.0001
2.0	1.0630	0.0641	1.0437	1.0283	1.0685	11.9	<0.0001
3.0	1.0815	0.1383	1.0460	1.0300	1.0725	42.6	<0.0001
4.0	1.0536	0.0306	1.0456	1.0341	1.0623	6.14	<0.0001
6.0	1.0462	0.0267	1.0406	1.0302	1.0498	2.02	<0.0001

Table 8 Summary Statistics Anderson-Darling Results for Degree Per Cell

DIV	Mean	Standard Deviation	Median	First Quartile	Third Quartile	Anderson-Darling Test Statistic	AndersonDarling p-value
0.5	1.94	0.998	2	1	2.5	2.16	<0.0001
1.0	2.03	1.08	2	1	3	2.22	<0.0001
1.5	2.65	2.26	2	1	4	5.92	<0.0001
2.0	2.94	2.09	2	1	4	6.48	<0.0001
3.0	4.53	2.89	4	2	6	6.04	<0.0001
4.0	4.94	3.18	4	3	7	4.01	<0.0001
6.0	8.70	3.23	8	6	10	0.364	0.405

Table 9 Kruskal-Wallis Test Results For All Features

Feature	χ^2	*p*-value
Average Segment Length Per Cell	88.9519	<0.0001
Average Relative Turning Angle Per Cell	7.7002	0.261

Number of Change Points Per Cell	234.2829	<0.0001
Total Length of All Neurites Per Cell	288.0794	<0.0001
Number of Neurites Per Cell	106.816	<0.0001
Average Tortuosity Per Cell	12.8792	0.045
Degree Per Cell	144.9114	<0.0001

Table 10 Dunn Test with Bonferroni Correction *p*-values for the Average Segment Length Per Cell (μm)

DIV	0.5	1.0	1.5	2.0	3.0	4.0
1.0	1.0000					
1.5	0.5123	1.0000				
2.0	0.0022	0.0380	0.2433			
3.0	0.0000	0.0000	0.0000	0.0265		
4.0	0.0000	0.0001	0.0003	0.3059	1.0000	
6.0	0.0000	0.0000	0.0000	0.0000	0.0067	0.0026

Table 11 Dunn Test with Bonferroni Correction *p*-values for the Average Relative Turning Angle Per Cell (°)

DIV	0.5	1.0	1.5	2.0	3.0	4.0
1.0	1.0000					
1.5	1.0000	1.0000				
2.0	1.0000	1.0000	1.0000			
3.0	1.0000	1.0000	1.0000	1.0000		
4.0	1.0000	1.0000	1.0000	1.0000	0.4895	
6.0	1.0000	1.0000	1.0000	1.0000	0.7938	1.0000

Table 12 Dunn Test with Bonferroni Correction *p*-values for the Number of Change Points Per Cell

DIV	0.5	1.0	1.5	2.0	3.0	4.0
1.0	1.0000					
1.5	0.7648	1.0000				
2.0	0.0009	0.0064	0.0463			
3.0	0.0000	0.0000	0.0000	0.0000		

4.0	0.0000	0.0000	0.0000	0.0000	0.0101	
6.0	0.0000	0.0000	0.0000	0.0000	0.0000	0.0213

Table 13 Dunn Test with Bonferroni Correction *p*-values for the Total Length of All Neurites Per Cell (μm)

DIV	0.5	1.0	1.5	2.0	3.0	4.0
1.0	1.0000					
1.5	0.3949	1.0000				
2.0	0.0001	0.0015	0.0225			
3.0	0.0000	0.0000	0.0000	0.0000		
4.0	0.0000	0.0000	0.0000	0.0000	0.0275	
6.0	0.0000	0.0000	0.0000	0.0000	0.0000	0.0045

Table 14 Dunn Test with Bonferroni Correction *p*-values for the Number of Neurites Per Cell

DIV	0.5	1.0	1.5	2.0	3.0	4.0
1.0	1.0000					
1.5	1.0000	1.0000				
2.0	1.0000	1.0000	1.0000			
3.0	0.0001	0.0001	0.0000	0.0000		
4.0	0.0000	0.0000	0.0000	0.0000	1.0000	
6.0	0.0000	0.0000	0.0000	0.0000	0.0043	0.0255

Table 15 Dunn Test with Bonferroni Correction *p*-values for the Average Tortuosity Per Cell

DIV	0.5	1.0	1.5	2.0	3.0	4.0
1.0	1.0000					
1.5	1.0000	1.0000				
2.0	1.0000	1.0000	0.4370			
3.0	1.0000	0.8980	0.0250	1.0000		
4.0	1.0000	1.0000	0.0542	1.0000	1.0000	
6.0	1.0000	1.0000	1.0000	1.0000	1.0000	1.0000

Table 16 Dunn Test with Bonferroni Correction *p*-values for the Degree Per Cell

DIV	0.5	1.0	1.5	2.0	3.0	4.0
1.0	1.0000					
1.5	1.0000	1.0000				

2.0	0.3069	0.4210	1.0000			
3.0	0.0000	0.0000	0.0000	0.0000		
4.0	0.0000	0.0000	0.0000	0.0000	1.0000	
6.0	0.0000	0.0000	0.0000	0.0000	0.0001	0.0010

Declarations

- **Authors' Contributions**
  Conceptualization: VAW, YJZ;
  Data Curation: (Lead) ASL, (Supporting) WC;
  Formal Analysis: ASL;
  Funding Acquisition: VAW, YJZ;
  Investigation: ASL;
  Methodology: ASL, VAW;
  Software: ASL;
  Supervision: VAW, YJZ;
  Visualization: ASL;
  Writing - Original Draft: ASL;
  Writing - Review & Editing: ASL, VAW, YJZ, (Supporting) WC;
- **Competing Interests**
  The authors have no competing interests to declare that are relevant to the content of this article.
- **Ethics Approval** Not Applicable
- **Consent to Participate** Not Applicable
- **Data Availability Statement**
  The data set presented in this work and the code used to analyze the data are available at https://doi.org/10.5281/zenodo.6415473 and https://doi.org/10.5281/zenodo.6415604, respectively.
- **Funding**
  This material is based upon work supported by the National Science Foundation Graduate Research Fellowship Program under Grant No. DGE1745016, the Faculty Early Career Development Program under Grant No. ECCS2044785 and the LEAP HI Program under Grant No. CMMI-1953323. The authors were also supported in part by a PITA (Pennsylvania Infrastructure Technology Alliance) grant and a PMFI (Pennsylvania Manufacturing Fellows Initiative) grant. Any opinions, findings, and conclusions or recommendations expressed in this material are those of the author(s) and do not necessarily reflect the views of the National Science Foundation.
- **Acknowledgements** We thank the anonymous reviewers for helpful comments on an earlier version of this manuscript.

References

Bicknell, B.A., Pujic, Z., Dayan, P., Goodhill, G.J. (2018, 6). Control of neurite growth and guidance by an inhibitory cell-body signal. *PLOS Computational Biology*, *14*(6), e1006218. Retrieved from https://doi.org/10.1371/journal.pcbi.1006218

Boulan, B., Beghin, A., Ravanello, C., Deloulme, J.-C., Gory-Faur´e, S., Andrieux, A., ... Denarier, E. (2020, 7). AutoNeuriteJ: An ImageJ plugin for measurement and classification of neuritic extensions. *PLOS ONE*, *15*(7), e0234529. Retrieved from https://doi.org/10.1371/journal .pone.0234529

Byrne, R.W., Noser, R., Bates, L.A., Jupp, P.E. (2009). How did they get here from there? Detecting changes of direction in terrestrial ranging. *Animal Behaviour*, *77*(3), 619–631. Retrieved from https://doi.org/10.1016/j.anbehav.2008.11.014

Conover, W.J. (1971). *Practical nonparametric statistics* (1st ed.). John Wiley & Sons, Inc.

Cuntz, H., Borst, A., Segev, I. (2007, 12). Optimization principles of dendritic structure. *Theoretical Biology and Medical Modelling*, *4*(1), 21. Retrieved from https://doi.org/10.1186/1742-4682-4-21

Deinhardt, K., Kim, T., Spellman, D.S., Mains, R.E., Eipper, B.A., Neubert, T.A., ... Hempstead, B.L. (2011, 12). Neuronal growth cone retraction relies on proneurotrophin receptor signaling through Rac. *Science Signaling*, *4*(202), ra82. Retrieved from https://doi.org/10.1126/ scisignal.2002060

Dinno, A. (2017). dunn.test: Dunn's test of multiple comparisons using rank sums [Computer software manual]. Retrieved from https://CRAN.R -project.org/package=dunn.test (R package version 1.3.5)

Dotti, C.G., Sullivan, C.A., Banker, G.A. (1988, 4). The establishment of polarity by hippocampal neurons in culture. *Journal of Neuroscience*, *8*(4), 1454–1468. Retrieved from https://doi.org/10.1523/jneurosci.08 -04-01454.1988

Ferrante, M., Migliore, M., Ascoli, G.A. (2013, 1). Functional impact of dendritic branch-point morphology. *Journal of Neuroscience*, *33*(5), 2156–2165. Retrieved from https://doi.org/10.1523/JNEUROSCI.3495 -12.2013

Ferreira Castro, A., Baltruschat, L., Stu¨rner, T., Bahrami, A., Jedlicka, P., Tavosanis, G., Cuntz, H. (2020, 11). Achieving functional neuronal dendrite structure through sequential stochastic growth and retraction. *eLife*, *9*. Retrieved from https://doi.org/10.7554/eLife.60920

Gillette, T.A., & Grefenstette, J.J. (2009, 9). On comparing neuronal morphologies with the constrained tree-edit-distance. *Neuroinformatics*, *7*(3), 191–4. Retrieved from https://doi.org/10.1007/s12021-009-9053-2

Gross, J., & Ligges, U. (2015). nortest: Tests for normality [Computer software manual]. Retrieved from https://CRAN.R-project.org/package=nortest (R package version 1.0-4)

Heumann, H., & Wittum, G. (2009, 9). The tree-edit-distance, a measure for quantifying neuronal morphology. *Neuroinformatics*, *7*(3), 179–90. Retrieved from https://doi.org/10.1007/s12021-009-9051-4

Ho, S.-Y., Chao, C.-Y., Huang, H.-L., Chiu, T.-W., Charoenkwan, P., Hwang, E. (2011, 12). NeurphologyJ: An automatic neuronal morphology quantification method and its application in pharmacological discovery. *BMC Bioinformatics*, *12*(1), 230. Retrieved from https://doi.org/10.1186/1471-2105-12-230

Jefferis, G.S., Potter, C.J., Chan, A.M., Marin, E.C., Rohlfing, T., Maurer, C.R., Luo, L. (2007, 3). Comprehensive maps of Drosophila higher olfactory centers: Spatially segregated fruit and pheromone representation. *Cell*, *128*(6), 1187–1203. Retrieved from https://doi.org/10.1016/ j.cell.2007.01.040

Kaech, S., & Banker, G. (2006, 12). Culturing hippocampal neurons. *Nature Protocols*, *1*(5), 2406–2415. Retrieved from https://doi.org/10.1038/nprot.2006.356

Kanari, L., Dl otko, P., Scolamiero, M., Levi, R., Shillcock, J., Hess, K., Markram, H. (2018). A topological representation of branching neuronal morphologies. *Neuroinformatics*, *16*(1), 3–13. Retrieved from https://doi.org/10.1007/s12021-017-9341-1

Kang, S., Chen, X., Gong, S., Yu, P., Yau, S., Su, Z., ... Shi, L. (2017, 12). Characteristic analyses of a neural differentiation model from iPSCderived neuron according to morphology, physiology, and global gene expression pattern.

Scientific Reports, *7*(1), 12233. Retrieved from https://doi.org/10.1038/s41598-017-12452-x

Khalil, R., Farhat, A., Dl otko, P. (2021, 5). Developmental changes in pyramidal cell morphology in multiple visual cortical areas using cluster analysis. *Frontiers in Computational Neuroscience*, *15*, 667696. Retrieved from https://doi.org/10.3389/fncom.2021.667696

Kim, K.-M., Son, K., Palmore, G.T.R. (2015, 12). Neuron image analyzer: Automated and accurate extraction of neuronal data from low quality images. *Scientific Reports*, *5*(1), 17062. Retrieved from https://doi.org/10.1038/srep17062

Kluyver, T., Ragan-Kelley, B., P´erez, F., Granger, B. (2016). Jupyter Notebooks – a publishing format for reproducible computational workflows. F. Loizides & B. Schmidt (Eds.), *Positioning and power in academic publishing: Players, agents and agendas* (pp. 87–90). IOS Press.

Krichmar, J.L., Nasuto, S.J., Scorcioni, R., Washington, S.D., Ascoli, G.A. (2002, 6). Effects of dendritic morphology on CA3 pyramidal cell electrophysiology: A simulation study. *Brain Research*, *941*(1-2), 11–28. Retrieved from https://doi.org/10.1016/S0006-8993(02)02488-5

Laturnus, S., Kobak, D., Berens, P. (2020, 10). A systematic evaluation of interneuron morphology representations for cell type discrimination. *Neuroinformatics*, *18*(4), 591–609. Retrieved from https://doi.org/10.1007/s12021-020-09461-z

Li, A., Barati Farimani, A., Zhang, Y.J. (2021, 12). Deep learning of material transport in complex neurite networks. *Scientific Reports*, *11*(1), 11280. Retrieved from https://doi.org/10.1038/s41598-021-90724-3

Li, A., Chai, X., Yang, G., Zhang, Y.J. (2019). An isogeometric analysis computational platform for material transport simulation in complex neurite networks. *Molecular & Cellular Biomechanics*, *16*(2), 123–140. Retrieved from https://doi.org/10.32604/mcb.2019.06479

Li, A., & Zhang, Y.J. (2022a, 3). Modeling intracellular transport and traffic jam in 3D neurons using PDE-constrained optimization. *Journal of Mechanics*, *38*, 44–59. Retrieved from https://doi.org/10.1093/jom/ ufac007

Li, A., & Zhang, Y.J. (2022b, 12). Modeling material transport regulation and traffic jam in neurons using PDE-constrained optimization. *Scientific Reports*, *12*(1), 3902. Retrieved from https://doi.org/10.1038/s41598 - 022-07861-6

Liao, A.S., Webster-Wood, V.A., Zhang, Y.J. (2021, 6 14-18). Quantification of neuron morphological development using the change-point test. *2021 summer biomechanics, bioengineering and biotransport conference.* Virtual. Retrieved from https://archive.sb3c.org/sb3c2021

Mainen, Z.F., & Sejnowski, T.J. (1996, 7). Influence of dendritic structure on firing pattern in model neocortical neurons. *Nature*, *382*(6589), 363–366. Retrieved from https://doi.org/10.1038/382363a0

Meijering, E., Jacob, M., Sarria, J.-C., Steiner, P., Hirling, H., Unser, M. (2004, 4). Design and validation of a tool for neurite tracing and analysis in fluorescence microscopy images. *Cytometry*, *58A*(2), 167–176. Retrieved from https://doi.org/10.1002/cyto.a.20022

Polavaram, S., Gillette, T.A., Parekh, R., Ascoli, G.A. (2014, 12). Statistical analysis and data mining of digital reconstructions of dendritic morphologies. *Frontiers in Neuroanatomy*, *8*, 138. Retrieved from https://doi.org/10.3389/fnana.2014.00138

Pool, M., Thiemann, J., Bar-Or, A., Fournier, A.E. (2008, 2). NeuriteTracer: A novel ImageJ plugin for automated quantification of neurite outgrowth. *Journal of Neuroscience Methods*, *168*(1), 134–139. Retrieved from https://doi.org/10.1016/J.JNEUMETH.2007.08.029

Powell, S.K., Rivas, R.J., Rodriguez-Boulan, E., Hatten, M.E. (1997, 2). Development of polarity in cerebellar granule neurons. *Journal of Neurobiology*, *32*(2), 223–236. Retrieved from https://doi.org/10.1002/(SICI)1097-4695(199702)32:2h223::AID-NEU7i3.0.CO;2-A

Python Core Team (2021). *Python: A Dynamic, Open Source Programming Language.* Python Software Foundation. Retrieved from https://www .python.org/

Qian, K., Pawar, A., Liao, A., Anitescu, C., Webster-Wood, V., Feinberg, A., ... Zhang, Y.J. (2022, 5). Modeling neuron growth using isogeometric collocation

based phase field method. *Scientific Reports*, *12*, 8120. Retrieved from https://doi.org/10.1038/s41598-022-12073-z

R Core Team (2021). *R: A Language and Environment for Statistical Computing.* Vienna, Austria: R Foundation for Statistical Computing. Retrieved from https://www.R-project.org/

RStudio Team (2021). *RStudio: Integrated Development Environment for R.* Boston, MA: RStudio, PBC. Retrieved from http://www.rstudio.com/

Rueden, C.T., Schindelin, J., Hiner, M.C., DeZonia, B.E., Walter, A.E., Arena, E.T., Eliceiri, K.W. (2017, 12). ImageJ2: ImageJ for the next generation of scientific image data. *BMC Bioinformatics*, *18*(1), 529. Retrieved from https://doi.org/10.1186/s12859-017-1934-z

Schaefer, A.T., Larkum, M.E., Sakmann, B., Roth, A. (2003, 6). Coincidence detection in pyramidal neurons is tuned by their dendritic branching pattern. *Journal of Neurophysiology*, *89*(6), 3143–3154. Retrieved from https://doi.org/10.1152/jn.00046.2003

Schindelin, J., Arganda-Carreras, I., Frise, E., Kaynig, V., Longair, M., Pietzsch, T., ... Cardona, A. (2012, 7). Fiji: An open-source platform for biological-image analysis. *Nature Methods*, *9*(7), 676–682. Retrieved from https://doi.org/10.1038/nmeth.2019

Sholl, D.A. (1953, 10). Dendritic organization in the neurons of the visual and motor cortices of the cat. *Journal of anatomy*, *87*(4), 387–406.

Su, C.-Z., Chou, K.-T., Huang, H.-P., Li, C.-J., Charng, C.-C., Lo, C.-C., Wang, D.-W. (2021, 10). Identification of neuronal polarity by nodebased machine learning. *Neuroinformatics*, *19*(4), 669–684. Retrieved from https://doi.org/10.1007/s12021-021-09513-y

Tahirovic, S., & Bradke, F. (2009, 9). Neuronal polarity. *Cold Spring Harbor Perspectives in Biology*, *1*(3), a001644-a001644. Retrieved from https://doi.org/10.1101/cshperspect.a001644

Tamariz, E., & Varela-Echavarr´ıa, A. (2015, 5). The discovery of the growth cone and its influence on the study of axon guidance. *Frontiers in*

Neuroanatomy, *9*, 51. Retrieved from https://doi.org/10.3389/fnana.2015.00051

Thermo Fisher Scientific (2018). *B-27 Plus Neuronal Culture System.* Life Technologies. Retrieved from https://www.thermofisher.com/document-connect/document-connect.html?url=https://assets.thermofisher.com/TFS-Assets/LSG/manuals/MAN0017319 B27 PlusNeuronalCultureSystem UG.pdf

Uylings, H.B.M., & van Pelt, J. (2002, 1). Measures for quantifying dendritic arborizations. *Network: Computation in Neural Systems*, *13*(3), 397–414. Retrieved from https://doi.org/10.1088/0954-898X 13 3 309

van Elburg, R.A.J., & van Ooyen, A. (2010, 5). Impact of dendritic size and dendritic topology on burst firing in pyramidal cells. *PLoS Computational Biology*, *6*(5), e1000781. Retrieved from https://doi.org/10.1371/journal.pcbi.1000781

Vetter, P., Roth, A., H¨ausser, M. (2001, 2). Propagation of action potentials in dendrites depends on dendritic morphology. *Journal of Neurophysiology*, *85*(2), 926–937. Retrieved from https://doi.org/10.1152/jn.2001.85.2.926

Waskom, M. (2021, 4). Seaborn: Statistical data visualization. *Journal of Open Source Software*, *6*(60), 3021. Retrieved from https://doi.org/10.21105/joss.03021

Zomorrodi, R., Ferecsk´o, A.S., Kov´acs, K., Kr¨oger, H., Timofeev, I. (2010, 5). Analysis of morphological features of thalamocortical neurons from

the ventroposterolateral nucleus of the cat. *The Journal of Comparative Neurology*, *518*(17), 3541–3556. Retrieved from https://doi.org/10.1002/ cne.22413